

# Elasticity and rheology of iron above 220 GPa and the nature of the Earth's inner core

Russell J. Hemley <sup>1,2</sup>, Baoheng L. Yao <sup>1</sup> & Anil K. Singh <sup>3</sup>

<sup>1</sup> *Geophysical Laboratory and Center for High Pressure Research, Carnegie Institution of Washington, 5251 Broad Branch Road, Y4S, Washington DC 24015, USA*

<sup>2</sup> *Consortium for Advanced Radiation Sources, University of Chicago, Chicago, Illinois 64637, USA*

<sup>3</sup> *Center for High Pressure Research, Mineral Physics Institute, State University of New York at Stony Brook, Stony Brook, New York 11794-2100, USA*

<sup>4</sup> *Materials Science Division, National Aerospace Laboratories, Bangalore 560017, India*

Recent numerical-modelling and seismological results have raised new questions about the dynamics and magnetism of the Earth's core. Knowledge of the elasticity and texture of iron at core pressures is crucial for understanding the seismological observations, such as the low attenuation of seismic waves, the low shear-wave velocity and the anisotropy of compressional-wave velocity. The density and bulk modulus of hexagonal-close-packed iron have been previously measured to core pressures by static and dynamic methods. Here we study, using radial X-ray diffraction and ultrasonic techniques, the shear modulus, single-crystal elasticity tensor, aggregate compressional- and shear-wave velocities, and orientation dependence of these velocities in iron. The inner core shear-wave velocity is lower than the aggregate shear-wave velocity of iron, suggesting the presence of low-velocity components or anelastic effects in the core. Observation of a strong lattice strain anisotropy in iron samples indicates a large (~24% compressional-wave anisotropy under the isostress assumption, and therefore a perfect alignment of crystals would not be needed to explain the seismic observations. Alternatively the strain anisotropy may indicate stress variation due to preferred slip systems.

Two radial X-ray diffraction (RXD) experiments (runs 1 and 2; see Fig. 1) were performed with diamond cells. Non-hydrostatic stress, a condition essential to the technique, was deliberately produced in the specimen by not adding a pressure medium. The stress state of the specimen compressed between two anvils is a superposition of the hydrostatic pressure

$$\sigma_p = (\sigma_3 + 2\sigma_1)/3 \quad (1)$$

and the differential stress components

$$t = \sigma_3 - \sigma_1 = 1.5(\sigma_3 - \sigma_p) \quad (2)$$

where  $\sigma_3$  and  $\sigma_1$  are axial and radial stresses, respectively<sup>17</sup>. A microfocus (4–10- $\mu\text{m}$  diameter) polychromatic X-ray beam, which passed through the Be gasket in the radial direction,

probed the lattice strain of the sample as a function of the angle ( $\psi$ ) to the diamond-cell axis<sup>15</sup>. At 21 pressures between 16 and 211 GPa, energy dispersive X-ray diffraction (EDXD) patterns containing ( $hkl$  notation) 100, 002, 101, 102, 110, 103, 112, 201 diffraction lines of hexagonal close packed (h.c.p.) iron, 111, 200, 220, 311, 222, 400, 331, 420, 422, 511 of gold, or 110, 200, 211, 220, 310, 222, 321, 400 of tungsten, were collected at 10° steps of  $\psi$  from 0° to 90°. The  $d$ -spacing varies linearly with  $\cos^2 \psi$ :

$$d(hkl) = d_p(hkl)[1 + (1 - 3\cos^2 \psi)Q(hkl)] \quad (3)$$

where the intercept  $d_p(hkl)$  denotes the  $d$ -spacing under  $\sigma_p$  and the slope  $Q(hkl)$  is the lattice strain under the uniaxial stress condition<sup>18,19</sup>.

In run 1, a separate gold layer was used as a standard for determination of  $t$  and shear modulus  $G$  of h.c.p. Fe. The axial stress is continuous across the interface between the gold and iron layers ( $\sigma_{3\text{Au}} = \sigma_{3\text{Fe}}$ ; subscripts denote the Au or Fe layer), that is

$$t_{\text{Fe}} = 1.5(\sigma_3 - \sigma_{p\text{Fe}}) = 1.5(\sigma_{p\text{Au}} - \sigma_{p\text{Fe}}) + t_{\text{Au}} \quad (4)$$

Now,  $t$  is related to  $G$  by

$$t = 6G\langle Q \rangle \quad (5)$$

where  $\langle Q \rangle$  denotes the average value of measured  $Q$  for all ( $hkl$ ) (ref. 15). The hydrostatic stress components,  $\sigma_{p\text{Au}}$  and  $\sigma_{p\text{Fe}}$ , were determined from the observed  $d_p(hkl)$  (equation (3)) and the equations of state of Au and Fe (refs 20, 21);  $G_{\text{Au}}$  was extrapolated from low-pressure data<sup>22,23</sup>. The aggregate compressional-wave speed ( $v_p$ ) and shear-wave speed ( $v_s$ ) of h.c.p. Fe are calculated from the bulk modulus  $K_{\text{Fe}}$  and  $G_{\text{Fe}}$ . In addition (run 3), the aggregate ultrasonic

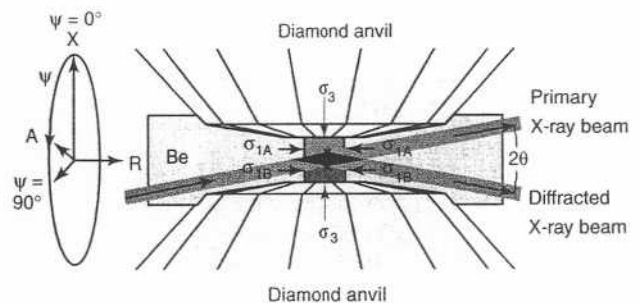


**Figure 1** Lattice strains of diamond-cell samples under uniaxial stress ( $\sigma_1$  and  $\sigma_3$ ) are obtained with radial X-ray diffraction (RXD) through a beryllium gasket. The subscripts A and B denote the sample and stress standard. The vertical scale of the sample region is expanded. In run 1, the specimen, which consisted of a 15- $\mu\text{m}$  (thickness) layer of an iron sample and a 3- $\mu\text{m}$  layer of a gold standard, was compressed in a 40- $\mu\text{m}$  (diameter) hole in a beryllium gasket between flat diamond anvils of 400- $\mu\text{m}$  diameter. In run 2, the specimen consisted of a 5- $\mu\text{m}$  iron and a 2- $\mu\text{m}$  tungsten layer in a 15- $\mu\text{m}$  hole in a Be gasket between bevelled diamond anvils (500- $\mu\text{m}$  outer diameter, 90- $\mu\text{m}$  inner diameter, 9.5° bevel angle). The diamond cell was mounted on a rotation stage with the diamond anvil axis (A) perpendicular to the rotation axis (R) which bisected the  $2\theta$  angle between incident and diffracted X-ray beams. The angle ( $\psi$ ) between A and the diffraction vector (X) was varied as the diamond cell rotated around the R axis.

**Table 1** Elasticity of h.c.p. Fe at 298 K and high pressures

P (GPa)	Density (g cm <sup>-3</sup> )	C <sub>11</sub> (GPa)	C <sub>12</sub> (GPa)	C <sub>33</sub> (GPa)	C <sub>13</sub> (GPa)	C <sub>44</sub> (GPa)	K (GPa)	G (GPa)	v <sub>p</sub> (km s <sup>-1</sup> )	v <sub>s</sub> (km s <sup>-1</sup> )	Run no.
16.5	9.00*										3
39	9.67*	504	244	493	254	271	351*	108	6.95	3.47	1
39	10.09	747	301	802	297	215	455	134	6.84	3.76	†
211	12.61‡	1303	637	1302	637	960	1071‡	224	7.86	4.72	†
211	12.80	1697	809	1799	757	421	1085	396	10.42	5.61	2
								445	10.54	5.90	†

Runs 1, 2 and 3 are results of this study. They are compared with values from first-principles calculations<sup>6</sup>. (The method and results of ref. 24 are similar to those of ref. 6.) Uncertainties for K and v<sub>p</sub>, 10% (runs 1 and 2), 2% (run 3); for C<sub>ij</sub>, G and v<sub>s</sub>, 20% (runs 1 and 2), 2% (run 3).

\*Ref. 21.

†Ref. 6.

‡Ref. 12.

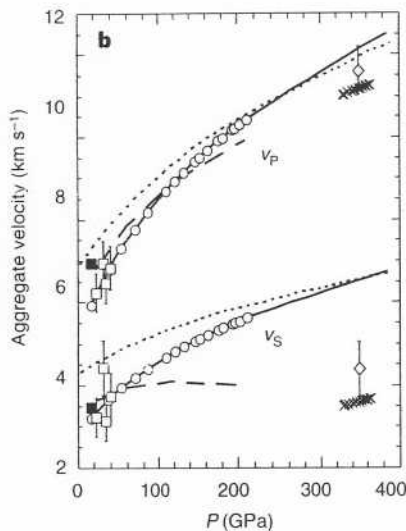
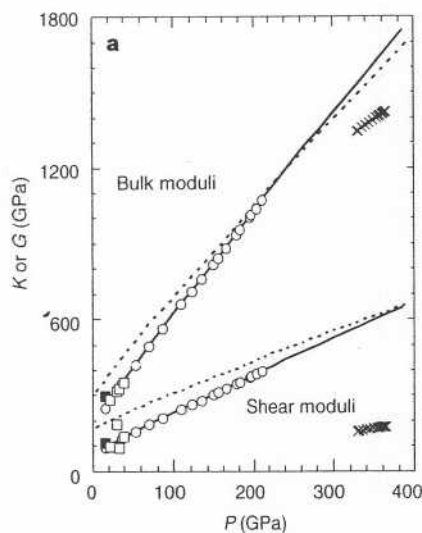


**Figure 2** Comparison of our results with theoretical and shock-wave studies, and with seismic observations<sup>25</sup> in the inner core (crosses). Parameters compared are shear moduli and bulk moduli (**a**), and aggregate  $v_S$  and  $v_P$  (**b**) of h.c.p. Fe. Filled squares, ultrasonic measurements with multi-anvil apparatus in run 3; open squares, RXD measurements in run 1; solid curves, extrapolation of X-ray data in run 2 based on  $K/G = 2.7$ ; short-dashed curves, first-principles calculations<sup>6</sup> for 298 K isotherm; long-dashed curves, shock-wave Hugoniot at high temperatures<sup>13,14</sup>. The solid curve was also used to calculate  $G$  and  $t$  for run 2 (open circles) for elasticity tensor estimations to 211 GPa. At 200 GPa, the differences between the Hugoniot values at 4407 K and the present 298 K values yield

temperature derivatives; for example,  $-dv_S/dT = 3.7 \times 10^{-4} \text{ km s}^{-1} \text{ K}^{-1}$  and  $-dv_P/dT = 0.9 \times 10^{-4} \text{ km s}^{-1} \text{ K}^{-1}$ . In comparison with other estimations based on theory of thermal and elastic properties<sup>20</sup>, this value of  $-dv_S/dT$  is high, and  $-dv_P/dT$  is low, possibly owing to the combined uncertainty in extrapolation of two data sets from entirely different studies (shock-wave and static compressions). If these derivatives are used for temperature correction of the solid curve to inner-core conditions, the resulting  $v_S$  and  $v_P$  of h.c.p. Fe at 6,000 K and 350 GPa (open diamonds in **b**) represent upper and lower bounds, respectively; that is, the differences between open diamonds and crosses is significant for  $v_S$ , but not for  $v_P$ .

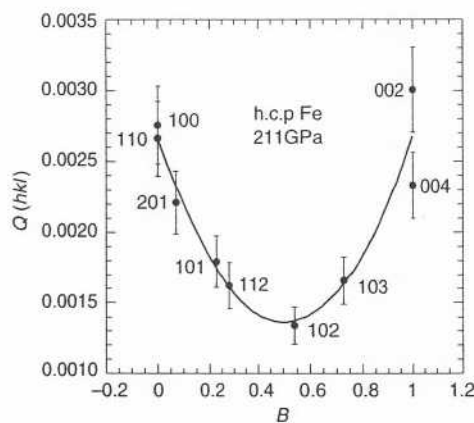


**Figure 3** The measured  $Q(hkl)$  of h.c.p. Fe at 211 GPa. This parameter follows a quadratic relation

$$Q(hkl) = m_0 + m_1 B + m_2 B^2 \quad (6)$$

where  $B = 3a^2/l [4c^2(h^2 + hk + l^2) + 3a^2]$ . Under isostress assumption, the parameters  $m_0$ ,  $m_1$  and  $m_2$  provide three independent linear equations for determination of elasticity tensors<sup>15,27</sup>.

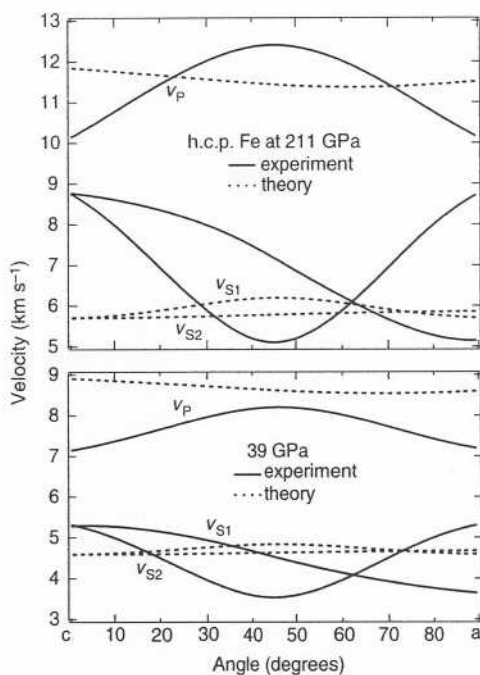


**Figure 4** Comparison of seismic-wave velocities from this work with values calculated from theory. The velocities ( $v_P$ ,  $v_{S1}$  and  $v_{S2}$ ) of single-crystal h.c.p. Fe depend on the wave propagation direction relative to the  $c$  axis of the crystal. Solid curves, this study with isostress assumption; dashed curves, first-principles theory<sup>6</sup>.

$v_P$  and  $v_S$  of h.c.p. Fe are measured directly at 16.5 GPa in a multi-anvil press<sup>16</sup>. All experiments were performed at 298 K.

The results from RXD (zero-frequency) and multi-anvil (ultrasonic-frequency) measurements are in good agreement, bracketing a wide frequency range including seismic waves. The observed  $K/G$  ratio of h.c.p. Fe is  $2.7(\pm 0.7)$  from the RXD at 20–39 GPa, and is  $2.68(\pm 0.1)$  from the ultrasonic measurement at 16.5 GPa. We extrapolate  $G_{Fe}$ ,  $t_{Fe}$ ,  $v_P$  and  $v_S$  to higher pressures based on a constant  $K/G$  of 2.7, and

compare the results with theoretical, shock-wave<sup>13,14</sup> and seismic values (Fig. 2). The  $K_{Fe}$ ,  $G_{Fe}$ ,  $v_P$  and  $v_S$  predicted by first-principles theory<sup>6,24</sup> are higher than the present values at low pressures, but the difference diminishes at higher pressures. Temperature derivatives of  $v_P$  and  $v_S$  are estimated from the differences between the Hugoniot data at high temperatures and the present static data at 298 K, and are used for estimation of  $v_P$  and  $v_S$  of h.c.p. Fe under the inner-core conditions<sup>25</sup> (Fig. 2b). The seismic  $v_S$  of the inner core is lower than the

pondering h.c.p. Fe value. If the softening of  $v_s$  represents possible (partial) partial melting effects" or partial melting, the observed shear values would tightly constrain the inner-core temperature near melting. The near-melting softening would also attenuate seismic. Alternatively, the observations may indicate the presence of additional low- $v_s$  phases in the inner core.

The RXD measurements also provide single-crystal elasticity information. Figure 3 shows that the  $Q(hkl)$  reaches a maximum at a (100, 110) and c (002) axes that is more than double the maximum of the  $Q(hkl)$  at the diagonals (112, 102, 103). This trend persists over the entire pressure range studied. The strong ( $hkl$ ) dependence of lattice strain reflects a strong elasticity anisotropy or an ( $hki$ ) dependence of stress<sup>11</sup>, which has little effect on the aforementioned estimates of averaged aggregate properties<sup>11</sup>, but which gives information on single-crystal properties. Elasticity tensors and the orientation dependence of  $v_p$ ,  $v_{s1}$  and  $v_{s2}$  (subscripts 1 and 2 denote two polarization directions) are calculated from parameters in equation (6) (see Fig. 3 legend) at the isostress limit<sup>11</sup>. Examples for h.c.p. Fe at 39 and 211 GPa are shown in Table I and Figs 2 and 4, and compared with values from first-principles theoretical predictions<sup>1</sup>. At 211 GPa (Fig. 3b), theories predicted a small  $v_p$  anisotropy (4% faster in the c than in the a direction) which requires a perfect alignment of h.c.p. Fe crystals (or a giant single crystal<sup>11</sup>) to account for the 4% inner-core  $v_p$  anisotropy. The present results obtained under the isostress assumption show a large  $v_p$  anisotropy (24% faster at 45° from c than along either the a or the c axis), which relieves the 'perfect alignment' textural constraint. Partial alignment of h.c.p. Fe crystals would be sufficient for the magnitude of inner-core anisotropy.

The isostress assumption for interpreting the data observed with our method has been confirmed experimentally for cubic phases of FeO and Fe (refs 15, 27). Its validity remains to be tested for hexagonal crystals. A strong ( $hkl$ ) dependence of  $v_s$  (that is, non-isostress) in the polycrystalline specimen may partially or fully account for the observed lattice strain anisotropy. Consequently the elasticity tensor can no longer be uniquely determined, but is only partially constrained by the lattice strain anisotropy in equation (6) with trade-offs among the values of the  $C_{ij}$  and textural parameters. For example, development of the basal-plane slip texture common in h.c.p. metals<sup>12</sup> could conceivably lower the  $\tau$  of grains with their c axis at 45° orientation. In such a case, the present observations at ultrahigh pressures, combined with elastic anisotropy information from theoretical estimates or single-crystal ultrasonic measurements at lower pressures, would yield geological information on single-crystal strength anisotropy and polycrystalline flow textures. Such information would affect our estimates of both elastic and anelastic anisotropies in the core<sup>29</sup>.

Much information on bulk properties at high temperatures and pressures, and single-crystal elasticity and strength anisotropy, may be obtained by integrating techniques complementary to the three-dimensional RXD measurements reported here. These include ultrasonic studies, which provide accurate and direct determination of velocities below 20 GPa, hydrostatic X-ray diffraction, which provides Lattice parameters and bulk moduli to multimegabar pressures, shock-wave experiments, which determine bulk elasticity along the high pressure-temperature Hugoniot, and  $ab$  initio calculations, which provide independent determinations of elasticity. The present integrated study reveals that the elasticity of the Earth's inner core may represent the low shear modulus of h.c.p. Fe dose to melting, or the existence of additional components with low shear-wave velocities but similar density to Fe. As well as perfectly aligned h.c.p. Fe, more complicated textures should be considered, including partial alignment of these phases. D

Received 4 March; accepted 17 September 1998.

Song, J. & Richards, P. C. Seismological evidence for differential rotation of the Earth's inner core. *Nature* 382, 21-224 (1996).

Su, W., Dzierwinski, A. N. I., & Leal, R. Planet within a planet: rotation of the inner core of Earth.

1. Song, J. & Richards, P. C. Seismological evidence for differential rotation of the Earth's inner core. *Nature* 382, 21-224 (1996).

2. Su, W., Dzierwinski, A. N. I., & Leal, R. Planet within a planet: rotation of the inner core of Earth. *Earth Planet. Inter.* 111, 1-11 (1998).

3. Chao, E. C. & Robert, P. II. Rural ion and magnetism in Earth's inner core. *Earth Planet. Inter.* 274, 188-193 (1996).

4. Kitting, K. & Bloch, H. An earth-like numerical dynamo model. *Nature* 389, 371-374 (1991).

5. Phipps, L. & O'Connell, R. J. Is the inner core of the Earth pure iron? *Nature* 325, 332-335 (1987).

6. Stairude, L. & Cohen, R. High-pressure elasticity of iron and anisotropy of Fe-rich inner core. *Earth Planet. Inter.* 267, 19-19 (1993).

7. Kikuchi, A. & Hillier, F. Solidity of the inner core of the Earth in iron, normal mode. *Nature* 234, 403-466 (1971).

8. Nesterov, D. & Hillier, F. Structure of the inner core inferred from observations of seismic shear waves. *Geophys. Res. Lett.* 8, 569-571 (1981).

9. Shearer, P. M., & Tost, K. Axi-symmetric Earth models and inner-core anisotropy. *Nature* 333, 23-23 (1991).

10. Chao, E. C. Anisotropy of the inner core from differential travel times of shear waves. *Earth Planet. Inter.* 356, 3119-3141 (1992).

11. Tromp, J. So-called anisotropy of the Earth's inner core from free oscillations. *Earth Planet. Inter.* 139, 1-13 (1991).

12. Sang, H.-K., Wu, Y., Chen, L. C., Shu, J.-F., & Leiferman, A. F. Static compression of iron to 300 GPa and Fe-Al alloy to 260 GPa: implications for the inner core. *Geophys. Res. Lett.* 21, 1199-1202 (1994).

13. Binnert, M. & Takahashi, F. (i) Phase-iransitions, Gruneisen-parameter, and elasticities for shocked iron between 0.1 and 400 GPa. *Geophys. Res. Lett.* 19, 435-439 (1992).

14. Dufv, F. S. C. Ahrens, T. J. in *High Pressure Research: Applications to Earth and Planetary Sciences* (eds Siren, Y. & Iijima, T.), 11-135. Springer-Verlag, Tokyo, 1992.

15. Singh, A. K., Mao, H.-K., Shu, J.-F., & Hemley, R. S. Estimation of single-crystal elastic moduli from polycrystalline x-ray diffraction at high pressure: Applications to FeO and iron. *Phys. Rev. Lett.* 80, 213-216 (1998).

16. Li, B., Jackson, I., & Liebermann, R. C. Elastic wave velocity measurement in multi-anvil apparatus at 10 GPa using ultrasonic interferometry. *Phys. Earth Planet. Inter.* 98, 79-91 (1996).

17. Felner, R. I. of af. N-rat imaging of stress and strain of diamond, and lungeen 41 megabar pressures. *J. Appl. Phys.* 76, 1242-1245 (1997).

18. Singh, A. K. & Dasgupta, C. The lattice strains in a specimen hexagonal silicite compressed nonhydrostatically in an opposed anvil high pressure setup-1. *Appl. Phys. Lett.* 75, 4936-4962 (1994).

19. Lehida, T., Funamori, N., & Tagi, T. Lattice strains in crystals under uniaxial stress field. *J. Appl. Phys.* 80, 7379-7461 (1996).

20. Anderson, D. L., Isaak, D. G., & Yamamoto, S. Anharmonicity and the contraction of stars for gold. *J. Appl. Phys.* 65, 1534-1531 (1989).

21. Leiferman, A. F., & Boll, P. A. The static compression of iron to 78 GPa (Fe with rare gas solids as pressure-transmitting media). *Phys. Rev. Lett.* 71, 4677-4684 (1986).

22. Simmons, C. & Wang, H. *Single Crystal Elastic Constants and Calculated Aggregate Properties* (NUT Press, Cambridge, MA, 1971).

23. Guinan, M. W. & 516 D, D. I. Pressure and temperature derivatives of the isotropic polycrystalline shear modulus for 65 elements-1. *Phys. Chem. Solid* 35, 1501-1512 (1974).

24. Suderliad, P., Moriarty, J. A., & Wills, J. H. First-principles theory of iron up to earth-core pressures: Structural, vibrational, and elastic properties. *Phys. Rev. B* 33, 14063-14072 (1996).

25. Zwickowski, A. a. - Anderson, D. L. Preliminary reference earth model. *Phys. Earth Planet. Inter.* 25, 297-336 (1981).

26. Tal, I. The volume dependence of elastic moduli and the Born-Durand melting hypothesis. *Phil. Mag.* 39, 151-161 (1991).

27. Singh, A. K., Balasingh, C., Mac, H.-K., Hemley, R. S., & 911 U.1. Analysis of lattice strains in iron under non-hydrostatic pressure. *J. Appl. Phys.* 83, 7567-7575 (1998).

28. Weak, H. R., Takeshita, T., & Leiferman, R. Development of texture and elastic anisotropy during deformation of jrcp metals. *Geophys. Res. Lett.* 15, 76-79 (1988).

29. Romanowicz, B., Li, X. D., & Doornik, I. Anisotropy in the inner core: on what it is due to low-order convection? *Science* 274, 963-966 (1996).

30. 51 cry, F. I. Theory of thermal and elastic properties of the lower mantle and core. *J. Geophys. Res.* 94, 219-245 (1989).

**Acknowledgements.** We thank I. Hu for technical help, L. Stixrude and R. E. Cohen for sharing theoretical data and discussions, T. Duff, for comments, and NSLS and APS for synchrotron beam time; the synchrotron facilities are supported by the DoE. This work was supported by the NSF.

Correspondence and requests for materials should be addressed to T.M. (e-mail: h1AO@qj.ciw.edu).

## Human longevity at the cost of reproductive success

Rudi G. J. Westendorp<sup>†</sup> & Thomas B. L. Kirkwood<sup>†</sup>

<sup>\*</sup> Section of Gerontology and Geriatrics, Department of General Internal Medicine, and Clinical Epidemiology, Leiden University Medical Centre CO-P, PO Box 9600, 2300 RC Leiden, The Netherlands

<sup>†</sup> Biological Gerontology Group, Department of Geriatric Medicine and The School of Biological Sciences, University of Manchester, 3.239 Stopford Building, Oxford Road, Manchester M13 9PT, UK

The disposable soma theory on the evolution of ageing states that longevity requires investments in somatic maintenance that reduce the resources available for reproduction<sup>1,2</sup>. Experiments in *Drosophila melanogaster* indicate that trade-offs of this kind exist in non-human species<sup>3-7</sup>. We have determined the interrelationship between longevity and reproductive success in *Homo*